Timing sequence design for a dual-frequency sounder in a flyby trajectory

V. Venkatesh *, A. Freedman *, D. Hawkins *, Y. Gim *, J. Martin *
* Jet Propulsion Laboratory, California Institute of Technology, Pasadena, CA.

***Abstract*—**
Recent advances in reconfigurable computing have led to a proliferation in on-board radar signal processing techniques such as synthetic aperture processing and digital beamforming. However, there have been relatively few investigations on automating radar operation using platform ephemeris. Reported studies to date have largely focussed on orbiter geometries with little change in range to target. In this work, we apply convex optimization methods to automate radar operation in a flyby geometry where the observation range spans nearly 2 orders of magnitude. Constraints are synthesized to allow for dual-frequency operation and adequate sampling of the Doppler spectrum. Performance of the designed timing sequences are benchmarked using Monte-Carlo simulations.

I. Introduction

Over the last few decades, advances in reconfigurable computing have led to significant improvements in radar system capabilities. While there has been a profileration in on-board digital signal processing techniques, there have been relatively few studies on automating radar operation using optimization methods. Early efforts on automating fire control radars focussed solely on pulse repetition frequency selection using algorithms that lacked the ability to optimize for multiple parameters [1]. Recent efforts on timing sequence design using numerical schemes allow for significantly more degrees of freedom. For example, TerraSAR-X mission investigations show remarkable improvements in data quality when the Pulse Repetition Frequency (PRF) is varied within the dwell in addition to the choice of mean PRF [2]. Other studies have applied numerical optimization methods to formation flying synthetic aperture radars [3]. In all these studies, variations in observation range have been relatively small. Furthermore, there has been no systematic effort devoted to numerical incorporation of hardware specifications such as switching times to incorporate resource sharing for multi-frequency operation.

This work focusses on timing sequence design for a spaceborne dual-frequency sounder with a flyby trajectory where radar altitude variations span almost 2 orders of magnitude [4]. Strong constraints are synthesized to allow the HF and VHF transmission windows to be interleaved thereby minimizing required peak prime power, while still maximizing signal to noise ratio (SNR) at each altitude. A weak constraint is employed to ensure adequate sampling of the Doppler spectrum for synthetic aperture formation. The following section outlines the methodology used to generate synthetic flyby trajectories and the convex optimization framework. Convex optimization [5] based timing sequence designs for various radar sounder modes for the Europa Clipper mission are then benchmarked with simulations of raw I/Q voltages at the antenna allowing for assessment of synthetic aperture imaging.

Corresponding author Email : vijay.venkatesh@jpl.nasa.gov .

II. Methodology

A. System description

NASA's flagship Europa Clipper mission [6] is an observing system of systems to probe Europa's ionosphere, map surface topology and characterize buried layers to discrimnate ice from potential liquid water bodies. The Radar for Europa Assessment and Sounding Ocean to Near-surface (REASON) is a dual-frequency radar sounder that allows a path to characterize Europa's sub-surface. Radar center frequencies are chosen to allow radio wave penetration of ice while also being sensitive to scattering from discontinuities in sub-surface permittivity [7] . However, natural radio emissions from Jupiter also compete with the frequncy band that has the highest ice penetration. To balance the susceptibility to Jovian radio emissions and ability to penetrate ice, a dual-frequency radar sounder design was arrived at. The lower 9 MHz frequency allows for deep ice penetration of the order of 30 km when the spacecraft is in a Jovian emission shadow. In addition, a 60 MHz frequency that is strategically placed outside the Jovian radio emission spectral band provides shallow ice penetration of the order of 3 km.

The nominal Europa Clipper mission will include over 40 flybys of Europa commencing radar observations at a 1000 km altitude and closest approach heights as low as 25 km. Given that range to Europa spans nearly 2 orders of magnitude, the choice of pulse repetition time must be dynamically varied to minimize dead time within the cycle [8]. Apriori spacecraft ephemeris knowledge is employed to minimize wait time between the transmit and receive windows. Otherwise stated, mutiple pulse trains can be transmitted together with the intention of assiging the receive window of transmit pulse n to correspond to ranging using the first pulse. Further, it is necessary that the HF and VHF transmit sequences to be appropriately interleaved to minimize requirements on peak prime power.

B. Optimization methodology

Herein, we parameterize a flyby with spacecraft altitude and velocity. The starting mantissa, duration of the flyby and

dwell time are additionally defined by the user. Assuming a perfectly linear trajectory with orbit determination errors, the observation geometry is then used to optimize timing sequence design for each point in the flyby using the following algorithm -

1) For each dwell within the flyby, the angle to limb is determined using the trigonometric relationship (1). Calculate Doppler velocities relative to the sounding range and nadir using (2)-(3). Subsequently, Doppler bandwidth for VHF is calculated using (4).

$$\theta_D = \cos^{-1} \frac{(1+\frac{h}{r})^2 + \frac{R^2}{r^2} - 1}{2\frac{R}{r}(1+\frac{h}{r})} \tag{1}$$

$$v_{doppSoundRange}(\lambda) = \frac{2(v_r \cos\theta_D + v_{tang} \sin\theta_D)}{\lambda} \tag{2}$$

$$v_{doppNadir}(\lambda) = \frac{2v_r \cos\theta_D}{\lambda} \tag{3}$$

$$B_{VHF} = 2\left|v_{doppNadir}(\lambda_{VHF}) - v_{doppSoundRange}(\lambda_{VHF})\right| \tag{4}$$

where $\lambda_{VHF} = 5\ m$. Since the received signal bandwidth is significantly larger at VHF than at HF, it suffices that we develop constraints to sample B_{VHF} adequately.

2) Denote the sub-surface of Europa as having a relative permittivity of ϵ_r. The propagation time in ice t_p is calculated as

$$t_p(d) = \frac{2d\sqrt{\epsilon_r}}{c} \tag{5}$$

where d is the sounding depth in meters, h is the spacecraft altitude above the surface of Europa and c is velocity of light in free space.

3) Note that we have defined a phrase "Cycle" Repetion Time (CRT) to bypass the conflated use of two pulses corresponding to the HF and VHF channels within the repetition time. The cycle definition employed herein is illustrated in Fig. 1. For each unique combination of cycle repetition time (T), chirp length (τ^{hf} and τ^{vhf} for the HF and VHF channels respectively) and number of pulses in the air (n), a cost function is computed using the following steps -

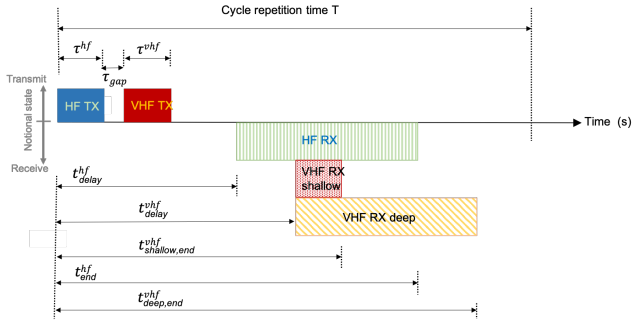

Fig. 1: Depiction of timing scheme used in the tool for radar timing sequence optimization. Here, "shallow" and "deep" refer to sounding depths of 3 and 30 km respectively.

a) Calculate the delay to the start of the HF receive echo (t^{hf}_{delay}) as

$$t^{hf}_{delay} = \frac{2h}{c} - nT. \tag{6}$$

The delay to the end of the HF receive window (t^{hf}_{end}) is given by

$$t^{hf}_{end} = t^{hf}_{delay} + \tau^{hf} + t_p. \tag{7}$$

b) Similarly, the receive delay to the start of the VHF receive echo (t^{vhf}_{delay}) is computed as

$$t^{vhf}_{delay} = \frac{2h}{c} + \tau^{hf} + \tau_{gap} - nT. \tag{8}$$

Although seperately computed for shallow and deep sounding depths, the time to the end of the VHF shallow window (t^{vhf}_{end}) can be compactly written as

$$hft^{vhf}_{end} = t^{vhf}_{delay} + \tau^{vhf} + t_p. \tag{9}$$

c) Assign a unique reward if the HF receive start time falls beyond the transmission window. This constraint is expressed as

$$J(\tau^{hf}, \tau^{vhf}, T, n) -- \ \forall \ \ t^{hf}_{delay} \geq \tau^{hf} + w\tau_{gap} + w\tau^{vhf}, \tag{10}$$

where w is a weight to quantify whether the VHF channel is in use. When the VHF channel is turned on, w is set to 1. The temporal gap between the HF and VHF transmission windows is expressed as τ_{gap}.

d) Assign a unique reward if the end of the HF receive window falls within the cycle repetition time. This can be stated as

$$J(\tau^{hf}, \tau^{vhf}, T, n) - = 2 \ \forall \ \ t^{hf}_{end} < T \tag{11}$$

e) Assign a unique reward if the VHF receive start time falls beyond the transmission window. This can be stated as

$$J(\tau^{hf}, \tau^{vhf}, T, n) - = 4 \ \forall \ \ t^{vhf}_{delay} \geq \tau^{hf} + w*\tau_{gap} + w\tau^{vhf}. \tag{12}$$

f) Assign a unique reward if the end of the VHF receive window falls within the cycle repetition time. This can be stated as

$$J(\tau^{hf}, \tau^{vhf}, T, n) - = 8 \ \forall \ \ t^{vhf}_{shallow,end} < T. \tag{13}$$

g) Assign a unique reward if the HF and VHF transmit duty cycles are less than the transmitter's 10 percent limit. In other words,

$$J(\tau^{hf}, \tau^{vhf}, T, n) - = 16 \ \forall \ \ \frac{\tau^{hf}}{T}, \frac{\tau^{vhf}}{T} \leq 0.1. \tag{14}$$

h) Assign a unique reward if the cycle repetition time allows for aqdeuate sampling of the VHF Doppler bandwidth. The quantity r denotes the ratio of the CRF to Doppler bandwidth and is determined using simulations. In other words,

$$J(\tau^{hf}, \tau^{vhf}, T, n) - = 32 \ \forall \ \ T > rB_{VHF}. \tag{15}$$

4) Identify solution sets S that correspond to the cost function minima as

$$S := \{ \ J(\tau^{hf}, \tau^{vhf}, T) = \min(J) \ \} \tag{16}$$

5) Within solution set S, choose chirp length and cycle repetition time to maximize the Signal-to-Noise Ratio (SNR) metric Q as

$$Q := \{ \ \frac{\tau^{hf}}{T} \ , \frac{\tau^{vhf}}{T} \ \} \tag{17}$$

The optimal timing sequence design is arrived at by maximizing Q as

$$Opt := \{ \ Q(\tau^{hf}, \tau^{vhf}, T, n) = \max_{\substack{\tau^{hf}, \tau^{vhf} \in S \\ T, n \in S}} (Q) \ \} \tag{18}$$

The final set Opt contains a unique timing sequence design τ^{hf}, τ^{vhf}, T and n that is optimal in the sense of the contraints defined herein.

III. Results

Herein, we design radar timing sequences using convex optimization by synthesizing contraints for transmit and receive window placement within a cycle. To avoid heuristic artifacts in gradient descent techniques [5], we compute the cost associated with fullfilling the constraints throughout the design space spanned by chirp length, cycle repetion frequency and pulses appended to the transmit burst. Although this approach for a global search of minimum cost is computationally inefficient, it allows multi-dimensional cost space visualizations to verify solution uniqueness. Fig. 2a and Fig. 2b show cuts of the cost function J about its global minimum. The set of potential design solutions S corresponding to minimum cost in equation (16) is indicated by the red boundary in Fig. 2a and Fig. 2b. Within the family of potential solutions S, Fig. 2c shows numerical computations of the SNR data quality metric Q defined by equation (17). Here, the metric Q is the product of chirp length and cycle repetition frequency, and maximizes SNR by virtue of ensuring highest average transmitted power within the cycle. Within the potential design solution candiates S, the design solution Opt is optimal in the sense of maximizing SNR and is indicated by the purple cross-hair in Fig. 2c. Fig. 3 shows optimized chirp lengths for the HF and VHF channels, along with cycle repetition times and pulses appended to the transmit burst in various parts of the flyby. Flyby input parameters, for which the timing sequence is optimized for, are shown in Fig. 3a. Note that discontinuities in the optimized timing sequence design are introduced when there is a change in the pulses in transit.

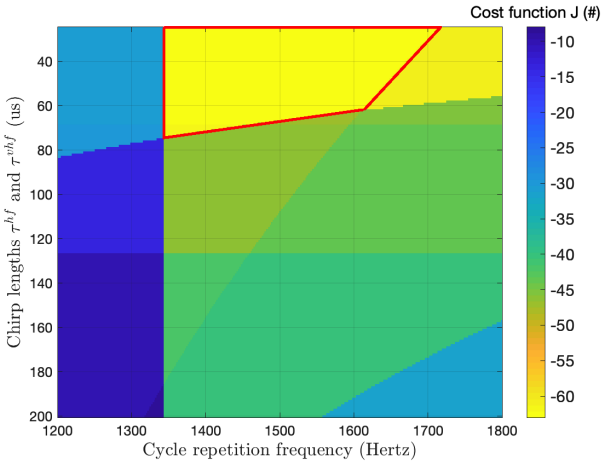

(a)

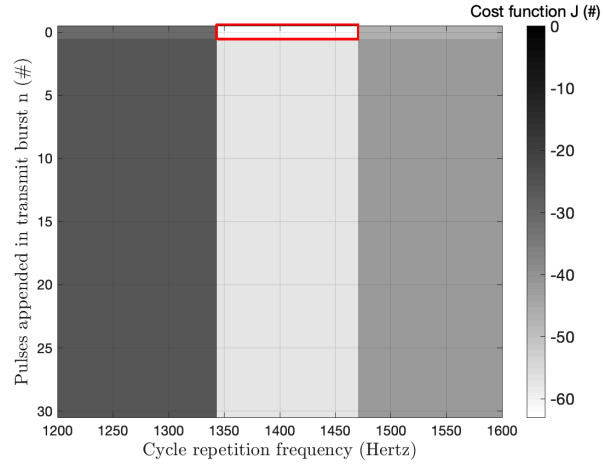

(b)

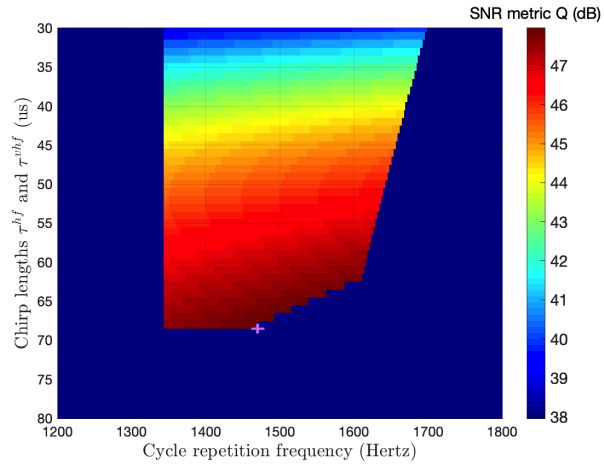

(c)

Fig. 2: Cost function for dual-frequency mode optimization at a closest approach altitude of 25 km, tangential velocity of 4 km/s and zero radial velocity. Receive windows front and back margins of 30 micro-seconds are employed to mitigate orbit determination errors. The VHF and HF channels have sounding depths of 3 km and 30 km respectively.

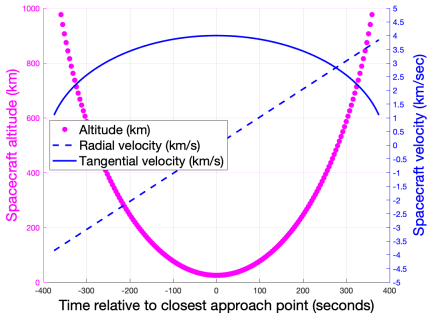

(a)

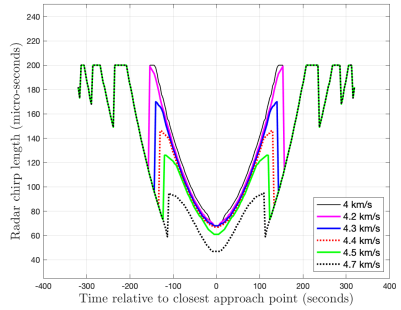

(b)

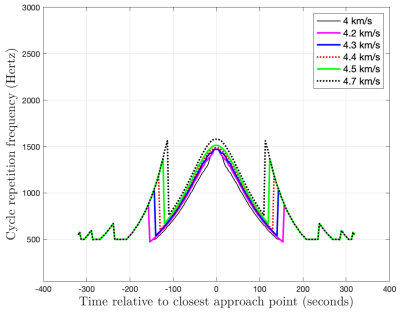

(c)

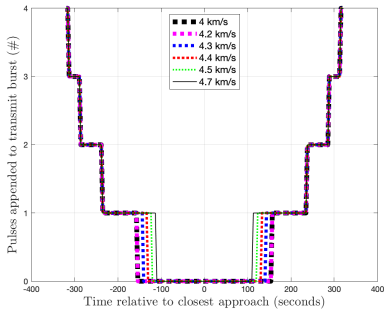

(d)

Fig. 3: Simulated chirp length and pulses appended in transmit burst for a flyby with closest approach at 25 km. A shallow VHF sounding mode of 3 km is employed. (a) Spacecraft altitude and velocity for flyby where timing sequence is subsequently optimized. (b) Optimized chirp length for flyby. (c) Optimized cycle repetition frequency for flyby. (d) Optimized appended pulses to transmit burst for flyby.

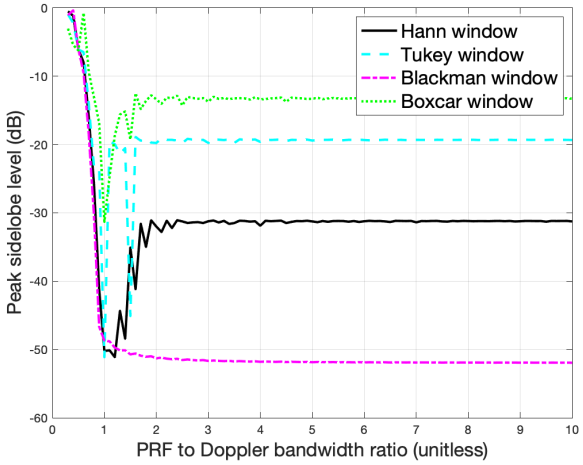

(a)

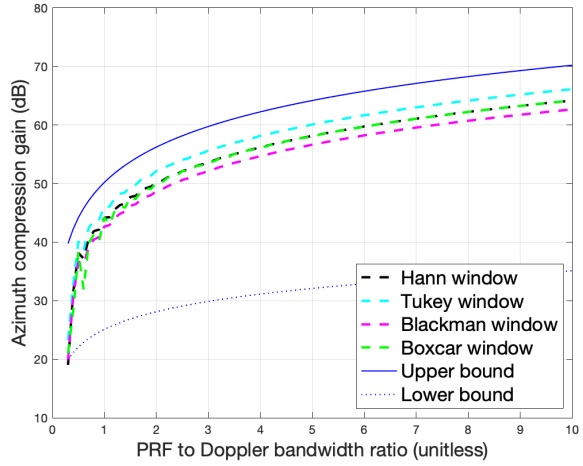

(b)

Fig. 4: Simulated peak sidelobe levels (a) and gain for synthetic aperture processing (b) using various PRF to Doppler bandwidth ratios. (a) The peak sidelobe levels for various windows converge to expected values when the Nyquist criterion is met or exceeded. (b) The upper bound denotes the coherent summation of the N pulses in the dwell, while the lower bound denotes incoherent summation. Note that when the PRF to Doppler bandwidth is very low, the insufficient sampling of the random process makes it appear incoherent.

Fig. 4 shows the simulated radar system performance for the timing sequence design arrived at in Fig. 3. Simulated raw I/Q voltages were used as inputs to synthetic aperture processing using a variety of data windows. In all these cases, Fig. 3a shows that the peak sidelobe level converged to the expected value when the Nyquist criterion for sampling the Doppler spectrum was met or exceeded (i.e. PRF to Doppler bandwidth ratio ≥ 2). Fig. 3b shows the azimuth compression gain for various data windows used in the synthetic aperture processor. The upper bound denotes the coherent summation of the N pulses in the dwell, while the lower bound denotes incoherent

summation. Note that when the PRF to Doppler bandwidth is very low, the insufficient sampling of the random process makes it appear incoherent. As the PRF to Doppler bandwidth increases, the azimuth compression gain approaches the coherent limit after accounting for the data loss due to windowing. The increase in azimuthal compressions gains become asymptotic beyond a PRF to Doppler bandwidth ratio of 0.8 for all the windows herein. Lastly, the azimuth compression gain is dependent on the choice of data window. As expected, boxcar windows have the highest azimuth compression gain, while the Blackman window has the lowest. Together, the fact that the simulated results in Fig. 4a and Fig. 4b are in line with expectations validates our simulation methodology. Fig. 5 shows the expected radar performance for the flyby. In Fig. 5a, we note a degradation in peak sidelobe level away from closest approach. To assist with interpreation, Fig. 5b shows that a decrease in along-track velocity causes this effect of increased azimuth sidelobe levels. In both these cases, the use of higher dwell times improved peak sidelobe levels.

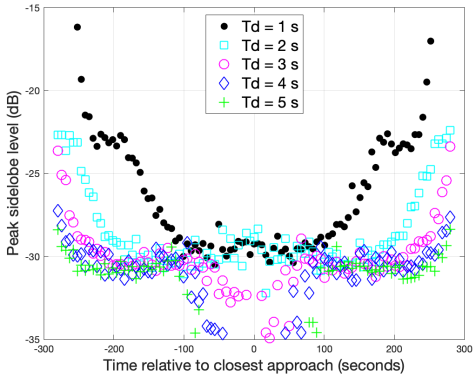

(a)

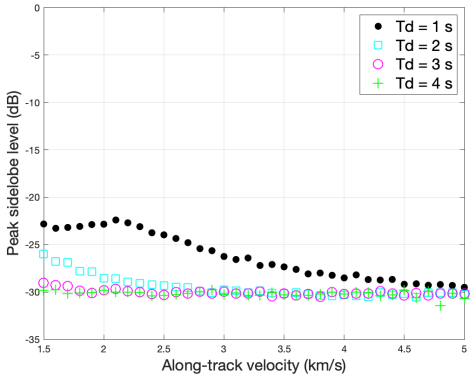

(b)

Fig. 5: Simulated peak sidelobe levels (a) and gain (b) for synthetic aperture processing for the flyby paramters in Fig. 3a. Fig. 5a shows that the peak sidelobe level degrades away from closest approach. To interpret this, Fig. 5b shows that a decrease in along-track velocity causes this effect of increased azimuth sidelobes while all other parameters are frozen. A dwell time of 2 s sufficient to ensure that peak sidelobe levels remain under 20 dB within the flyby.

IV. Summary

Herein, convex optimization techniques were applied to design timing sequences for a spaceborne dual-frequency sounder in a flyby trajectory. Strong constraints were synthesized to allow the HF and VHF transmission windows to be interleaved thereby minimizing the required peak prime power. Weak constraints were syntesized to ensure adequate sampling of the Doppler spectrum. Design performance was benchmarked with simulations of raw I/Q voltages at the antenna allowing for assessment of synthetic aperture imaging.

The designed timing sequence had three degrees of freedom - namely chirp length, cycle repetition frequency and pulses appended to transmit burst. While the chirp repetition frequency roughly followed the VHF Doppler bandwidth as a function of altitude, discontinuities were observed when there was a change in the number of pulses in transit. This discountinuos behaviour also extended to chirp length designs using convex optimization. Notwithstanding, numerical simulations showed that the impact of discontinuities in timing sequence designs on synthetic aperture imaging was rather muted when the Doppler spectrum was adequately sampled. Simulations also revealed that a reduction in along track velocity away from closest approach caused an increase in peak sidelobe level. The use of longer dwell times mitigated this effect.

References

[1] P. Davies and E. Hughes, "Medium prf set selection using evolutionary algorithms," vol. 38, no. 3, pp. 933–939, Jul. 2002.

[2] M. Villano, G. Krieger, M. Jager, and A. Moreira, "Staggered SAR : Performance analysis and experiments with real data," *IEEE Trans. Geoscience Remote Sensing*, vol. 55, pp. 6617–6637, Nov. 2017.

[3] M. Graziano, A. Renga, M. Grasso, and A. Moccia, "Prf selection in formation flying sar : Experimental verification on sentinel-1monostatic repeat pass data," *Remote Sensing*, vol. 38, pp. 933–939, Jul. 2002.

[4] K. Scanlan, D. Young, G. Steinbrugge, S. Kempf, C. Grima, and D. Blankenship, "Delay doppler sar focussing and quantitative quality control of the radar for europa assessment and sounding : ocean to near-surface (reason) data product," *IEEE Journal of selected topics in applied earth observations and remote sensing*, vol. 14, pp. 4352–4369, Apr. 2021.

[5] S. Boyd and L. Vandenberghe, *Convex optimization*. Cambridge university press, 2004.

[6] S. Howell and R. Pappalardo, "Nasa's europa clipper - a mission to a potentially habitable ocean world," *Nature communications*, vol. 11 (1311), Mar. 2020.

[7] R. Beauchamp, D. Arumugam, M. Burgin, J. Bush, A. Khazendar, Y. Gim, and A. Alanezi, "Can airborne ground penetrating radars explore groundwater in hyper-arid regions," *IEEE Access 6*, pp. 27 736–27 749, Mar. 2020.

[8] R. D. West, Y. Anderson, R. Boehmer, P. C. L. Borgarelli, C. Elachi, G. H. Y. Gim, S. Henseley, M. Janssen, W. T. K. Johnson, K. Kelleher, R. Lorenz, S. Ostro, L. Roth, S. Shaffer, B. Stiles, L. W. S. Wall, and H. Zebker, "Cassini radar sequence planning and instrument perfromance," *IEEE Trans. Geoscience Remote Sensing*, vol. 49, no. 6, Jul. 2009.